EUROPEAN JOURNAL OF COMPUTATIONAL MECHANICS, 2016
VOL. 25, NO. 5, 359–387
http://dx.doi.org/10.1080/17797179.2016.1240535

Taylor & Francis
Taylor & Francis Group

Drag reduction by a multi-point optimised hybrid flow control method for two supercritical airfoils

A. Nejati and K. Mazaheri

Center of Excellence in Aerospace Systems, Sharif University of Technology, Tehran, Iran

ABSTRACT

Shock control bump (SCB), suction and blowing are three flow control methods used to control the shock wave/boundary layer interaction to reduce the resulting wave drag in transonic flows. An SCB uses a small local surface deformation to reduce the shock wave strength, while the suction decreases the boundary layer thickness and the blowing delays the flow separation. Here, we will use a multi-point continuous adjoint optimisation scheme to find the optimum design of suction and blowing separately or together, or with the SCB, on two supercritical airfoils, i.e. RAE-5225 and RAE-2822, for a wide range of off-design transonic Mach numbers. The RANS flow equations are solved using the Roe's averages scheme. The independent usage of the SCB, the suction and the blowing methods has resulted in the average aerodynamic performance improvement of, respectively, 11.7, 4.16, and 4.21%, with respect to the clean RAE-5225 airfoil and for the RAE-2822 these numbers are 11.1, 4.04, and 6.61%, respectively. The simultaneous usage of suction with blowing results in 8.61% improvement of the average aerodynamic efficiency for the RAE-5225, while this increase is 7.63% for the RAE-2822. The hybrid usage of all three methods improves the average aerodynamic performance by 17.7% for the RAE-5225 and 22.1% for the RAE-2822. It is shown that the suction does not change the shock wave position significantly, but the blowing moves it forward, and reduces or removes the separated region after the shock wave or the SCB.

ARTICLE HISTORY
Received 11 March 2016
Accepted 21 September 2016

KEYWORDS
Supercritical airfoil; shock wave; drag reduction; flow control methods; multi-point adjoint optimisation

1. Introduction

Nowadays one of the most challenging objectives in civil aircraft design is the increase in velocity in the transonic flow regime. It requires design of high aerodynamic performance wings for this flight condition. This is restricted by the initiation of the strong shock wave, which will interact with the boundary layer, and results in the growth of the boundary layer thickness and increases the

CONTACT A. Nejati a_nejati@alum.sharif.edu

possibility of flow separation with undesirable aerodynamic and control consequences. Usually aerodynamic efficiency is a function of the drag coefficient, and drag reduction results in the increase in the aerodynamic efficiency. In the design of a civil aircraft, considering operational costs which are mostly due to the fuel cost, and also environmental issues and pollution control protocols, the drag reduction is of the highest importance.

In the project Euro-Shock (Milholen & Lewis, 2005; Patzold, Lutz, Kramer, & Wagner, 2006), European research institutes have recommended various methods to reduce the wave drag which are called flow control methods. The flow control methods in transonic regime to improve the shock wave/boundary layer interaction (SWBLI) are of great importance, especially at off-design high Mach numbers which is very sensitive to shape or flow variations. Many different methods are introduced during the last two decades for flow control in transonic flow regime, including adaptive aerodynamic surfaces. These schemes not only reduce the drag coefficients and improve the aerodynamic performance, but also increase the lift coefficient, delay buffet phenomenon and increase manoeuvrability (Evans, Hynes, Norman, & Thomason, 1984). To control the effects of shock waves, many of these flow control methods are implemented, e.g. blowing, suction, vortex generators, shape changes, oscillation control and usage of cavity or porous surfaces at the shock wave location (Stanewsky, Delery, Fulker, & de Matteis, 2002). Ashill, Fulker, and Shires (1992) in 1992 introduced local surface deformation or shock control bump (SCB), to reduce drag force induced by shock waves in transonic flow. Many researchers have shown that the SCB is more effective than other flow control methods, e.g. cavity, suction, blowing, surface cooling or heating (Bhattacharjee, Ahsan, Saha, & Mohammad, 2007; Lee, Bugeda, Periaux, & Onate, 2013; Qin, Zhu, & Shaw, 2004). Some people have recommended hybrid usage of SCB with boundary layer suction (Yagiz, Kandil, & Pehlivanoglu, 2012) or with simultaneous suction and blowing (Vadillo, Agarwal, & Hassan, 2004).

The standard optimisation scheme is one-point optimisation, i.e. the optimised shape is only optimum in the reference or design point, but may not be optimal in off-design points. However, the multi-point optimisation will result in a shape that is not optimum in any of flight conditions, but its overall performance is optimum in the defined range of flight conditions. In 2007, Jameson, Leoviriyakit, and Shankaran (2007) used adjoint equations to formulate automatic multi-point optimisation along with numerical solution of flow equations.

Authors have recently used the single-point evolutionary optimisation scheme and also the multi-point adjoint gradient-based method to improve the application of the SCB for better aerodynamic performance of two transonic airfoils under constant angle of attack condition (Mazaheri, Kiani, Nejati, Zeinalpour, & Taheri, 2015; Mazaheri, Nejati, kiani, & Taheri, 2015). We have also studied the robust optimisation of 2D SCBs and the multi-point optimisation of 3D SCBs for two different 3D wing configurations (Mazaheri, Nejati, & Kiani, 2016). We have shown that the three-dimensional SCBs have a better overall performance in

comparison with the 2D configuration. Moreover, we have optimised the hybrid usage of suction with SCB and blowing with SCB in constant lift coefficient condition (Mazaheri & Nejati, 2015).

In this article, we will first study the separate application of suction and blowing for two supercritical airfoils, i.e. RAE-5225 and RAE-2822 airfoils, and will find their optimum design and performance. Next, we will study the hybrid usage of suction and blowing, with and without the SCB, and will use our multi-point optimisation scheme to find their optimum design and performance. Our main focus in this article is on the comparison of different flow control methods used alone and all together using a multi-point optimisation strategy. To analyse the flow field, we use a finite volume method to solve RANS equations. To compute the convective fluxes in our numerical scheme, we have used Roe approximations (Blazek, 2005) with the second order of accuracy, and have used the Menter form of the K–ω turbulence model (Menter & Rumsey, 1994). The steepest decent algorithm is used in our continuous adjoint optimisation scheme (Rao, 1996). The main contributions of this article are summarised as follows.

- Analysis of the near-field viscous interactions of the suction and the blowing with the boundary layer.
- Analysis of the outer flow inviscid interactions of the suction and the blowing with the shock wave, and study of the wave pattern over the transonic airfoil.
- The multi-point adjoint optimisation of simultaneous suction and blowing for drag reduction and comparison of their performance with their independent usage.
- Comparison of performance of different flow control configurations for two different airfoils with different flight conditions.
- The multi-point adjoint optimisation of hybrid SCB/suction/blowing flow control for drag reduction.

2. Flow control methods

SCB, suction and blowing are known flow control methods. The SCB geometry and its position are designed so that a number of isentropic compression waves are formed when the flow moves upward of the bump. Passing through these isentropic compression waves, flow velocity is gradually reduced and the pressure is gradually increased (instead of sudden changes). Downhill of the bump, we have some expansion waves, and then the flow passes through a weakened shock wave (Figure 1). The schematic of suction and blowing geometry are shown in Figure 2. The main purpose of using suction is to remove the low-energy boundary layer flow, while using blowing we energise the boundary layer, and enhance the velocity profile. This will delay occurrence of the inflexion point and separation from the wall.

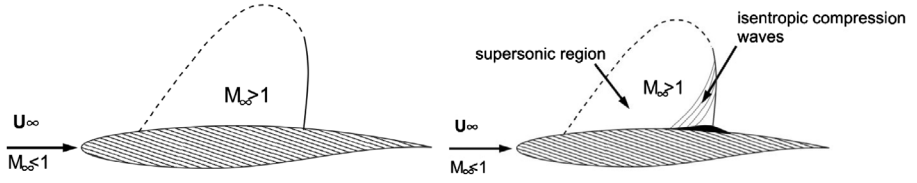

Figure 1. Effect of the SCB.

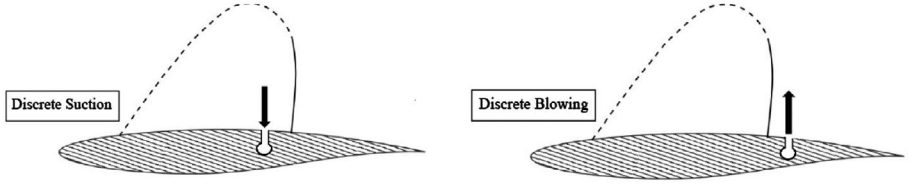

Figure 2. Schematic of the suction and the blowing over a supercritical airfoil.

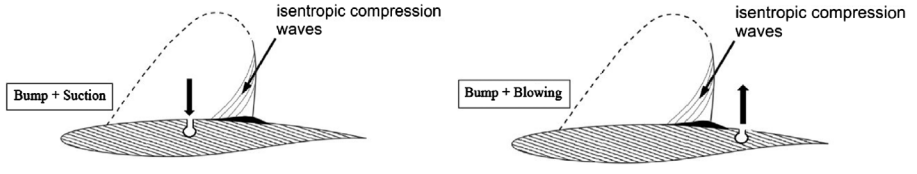

Figure 3. Schematic of the suction and the blowing over a bumped supercritical airfoil.

Balleur et al. at ONERA (Balleur, Girodroux-Lavigne, & Gassot, 1999) showed that suction upstream of the shock wave for an RAE-5225 airfoil may reduce the total drag coefficient by 5.1%. Other researchers at Karlsruhe University in Germany (Stanewsky et al., 2002) used a DRA-2303 airfoil to find the effect of suction location and mass flow on its performance. They showed that reductions in drag coefficients are between 2.5 and 4.9%. In 2006, Vadillo et al. (2004) used numerical simulation to study effects of location, mass flow, amplitude and frequency of a flow jet used for blowing after the shock wave, to improve lift, drag and bending moment coefficients in a transonic flow.

Obviously appropriate combination of these two different flow control schemes may improve the aerodynamic performance. Geometrical schematic of this hybrid method is shown in Figure 3. The performances of hybrid suction/SCB and hybrid blowing/SCB are investigated in (Qin et al., 2004; Yagiz et al., 2012). In another work, Birkemeyer has studied addition of upstream suction to SCB at different angles of attack for a swept back ADIF wing (Birkemeyer, 1999). Also Qin, Zhu, and Ashill (2000) have used parametric study to investigate hybrid effects of SCB, suction and blowing for an RAE-5243 airfoil. They showed that suction in upstream of the shock wave and blowing close to the trailing edge may further improve the aerodynamic performance of the SCB. Yagiz et al. (2012) have also

investigated effect of flow control schemes to improve performance of RAE-5243. Using gradient optimisation algorithms, they have been able to decrease the drag coefficient by 3.49% and to increase the lift coefficient by 5.04%. We will show in this article that with a better optimisation strategy much better results which are valid for a wider range of flight conditions may be achieved.

3. Problem definition

In this article, we will first consider multi-point optimisation of suction or blowing schemes to the clean airfoils, and then we will do multi-point optimisation of the hybrid flow control, i.e. suction along with blowing and all mentioned flow control methods together.

For a single-point optimisation, only one flight condition is considered. For a typical airfoil in constant angle of attack, the total drag coefficient (Cd_t) is almost constant for a wide range of subsonic free stream velocities. This will readily increase by approaching to the drag divergence Mach number. Strong shock waves and their interaction with boundary layer are the drivers of rapid increase in drag coefficient, which is called 'drag divergence'.

In this study, two supercritical airfoils, RAE-5225 and RAE-2822 (see Tables 1 and 2) are studied. The choice of the off-design conditions is based on cases numerically studied earlier by Tian, Liu, and Feng (2011). He has also used four points which sound practically appropriate. The procedure is based on the conventional procedures in wind tunnels, in which they use constant free-stream stagnation conditions and the model angle of attack is fixed but the flow Mach number changes. Tian has used a rage of Mach numbers between .73 and .76, but we have increased this range to .74 up to .77 for the RAE-5225 and .75 up to .79 for the RAE-2822, to consider initiation and interaction of stronger shock waves with the bump. The drag divergence diagrams for these two airfoils are given in Figure 4. To consider effectivity of flow control methods in higher angles of attack, we have considered a higher angle of attack for the RAE-5225 airfoil in comparison with the AE-2822 airfoil.

Table 1. Flight conditions for the RAE-5225 airfoil, $Rey_\infty = 6.1 \times 10^6$ and $\alpha = 3.0$.

Flight condition	*M*	*Cl*	*Cd*	*L/D*
1	.74	.692	.0178	38.9
2	.75	.678	.0209	32.4
3	.76	.645	.0242	26.6
4	.77	.598	.0274	21.8

Table 2. Flight conditions for the RAE-2822 airfoil, $Rey_\infty = 7.6 \times 10^6$ and $\alpha = 1.5$.

Flight condition	*M*	*Cl*	*Cd*	*L/D*
1	.75	.554	.0133	41.6
2	.76	.542	.0160	33.9
3	.78	.487	.0223	21.8
4	.79	.446	.0251	17.8

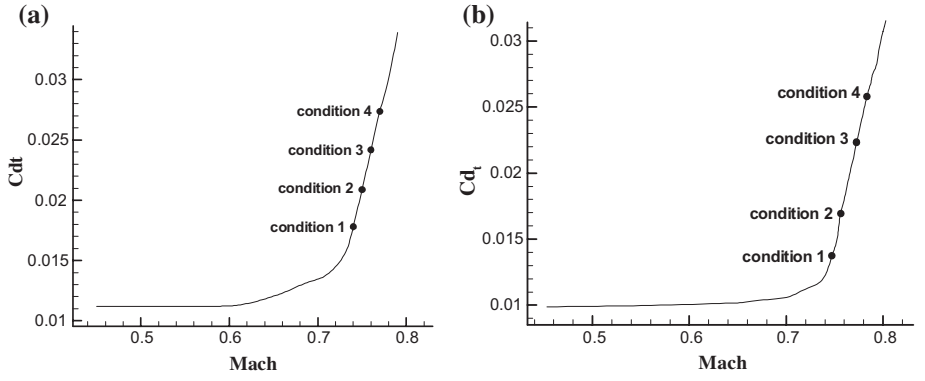

Figure 4. The drag divergence diagram for (a) the RAE-5225 airfoil at $\alpha = 3.0°$ and (b) the RAE-2822 airfoil at $\alpha = 1.5°$.

There are two different optimisation strategies with different motivations. One is optimisation under constant angle of attack, as followed in (Koenig, Paetzold, Lutz, & Kraemer, 2007). The motivation here is to increase payload of an existing aircraft without major change in wing installation angles. In this strategy as explained in (Koenig et al., 2007), after optimisation, the total angle of attack is changed in flight if the previous lift coefficient is required. The other strategy is optimisation under constant *Cl* (variable angle of attack), which is not followed here.

4. Optimisation algorithm

Optimisation algorithms are categorised as gradient and non-gradient-based algorithms. In the former, the gradients of objective function with respect to the design variables play an important role in the optimisation process. In this research, the gradient-based steepest descent algorithm is used to find the optimum point and the adjoint method is also used to find the gradient of the objective function. Therefore, minus of the gradient vector shows the optimisation direction. The optimisation process begins by guessing the initial value of design variables. Then in an iterative process, we proceed through the maximum descent direction of the cost function to reach to an optimum point. (For details of the steepest descent algorithm and the adjoint method, please see Rao [1996], Anderson and Venkatakrishnan [1997], and Mazaheri and Zeinalpour [2015]). To apply geometrical constraints to our design parameters, we have used external penalty function scheme based on Rao (1996).

5. Flow governing equations and boundary conditions

The integral form of the governing equations for each cell is introduced in Equation (1). In this equation, $\mathbf{U}$, $\mathbf{f}_c$, $\mathbf{f}_v$ stand for the conservative variable vectors, the convection flux vector and the viscous flux vector, respectively.

$$\frac{\partial}{\partial t}\int_{\Omega}\vec{\mathbf{U}}\,\mathrm{d}\Omega+\oint_{\partial\Omega}\left(\vec{\mathbf{f}}_c-\vec{\mathbf{f}}_v\right)\mathrm{ds}=0 \tag{1}$$

Finite volume method is used for flow field discretisation. Flux across each cell face is approximated using Roe flux difference splitting method, $\mathbf{f}_c$ (convection flux vector) is computed for each cell face by Equation (2).

$$\left(\vec{\mathbf{f}}_c\right)_{I+1/2}=\frac{1}{2}\left[\vec{\mathbf{f}}_c(\vec{\mathbf{U}}_R)+\vec{\mathbf{f}}_c(\vec{\mathbf{U}}_L)-\left|\bar{\mathbf{A}}_{Roe}\right|_{I+1/2}\left(\vec{\mathbf{U}}_R-\vec{\mathbf{U}}_L\right)\right] \tag{2}$$

$|\mathbf{A}_{Roe}|_{I+1/2}$ is Jacobian of the convection flux vector. For more details about the Roe averaged variables, please see Mazaheri, kiani et al. (2015). The second order of accuracy is achieved by the MUSCL scheme (Blazek, 2005). Also, the equations for K–ω turbulence modelling in the flow field are based on Menter and Rumsey (1994). The free stream conditions are applied as the far-field boundary conditions. A no-slip condition is used on the airfoil surface and the channel walls. Over the suction or the blowing regions, the average velocity of the inlet/outlet velocity profile is defined as:

$$U_{ave}=\frac{m^{\bullet}}{\sum\limits_{L_{\text{suction}}}\rho_{sb}\Delta s} \tag{3}$$

where subscript *sb* denotes the channel inlet, and the non-dimensional mass flow is defined as:

$$C_Q=\frac{m^{\bullet}}{\rho_{\infty}U_{\infty}c} \tag{4}$$

In the above, c is the chord. For the suction, C_Q is negative and it is positive for the blowing. In the exit of channel, pressure outlet or inlet boundary condition is implemented.

6. Validation of the flow solver

A 2D finite volume Navier–Stokes RANS solver which is developed at CEAS[1] is used as the flow solver (Ramezani & Mazaheri, 2009). To validate it, the transonic flow around the supercritical RAE-2822 airfoil is simulated on a 4 × 3.4 GHz CPU. The flow conditions are Mach number $M_{\infty}=.73$, Reynolds number $Rey_{\infty}=6.5\times10^6$ and angle of attack $\alpha=2.31°$. The generated C-type mesh is shown in Figure 5. After a grid independence study, an acceptable grid is chosen that includes 400 nodes on the airfoil surface, 100 nodes in the wake region and 70 nodes in the vertical direction (total nodes = 42,000). The aerodynamic coefficients and the surface pressure and the skin friction coefficient distribution compared with data

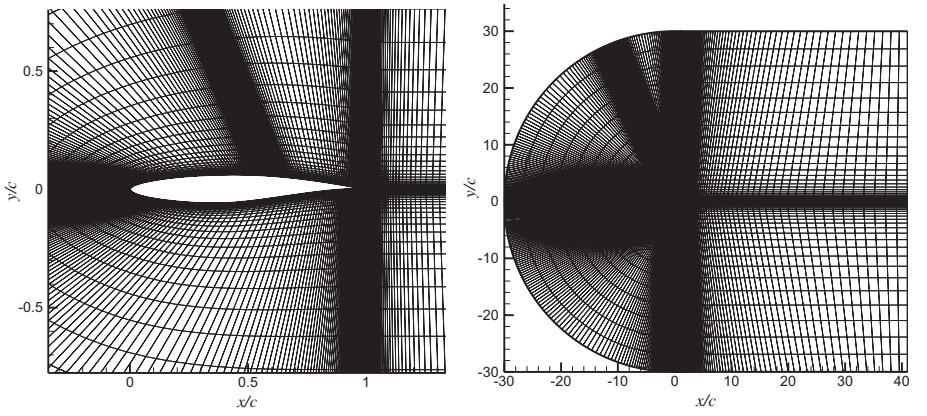

Figure 5. A sample grid generated around the RAE-2822 airfoil.

Table 3. Validation of numerical scheme for the RAE-2822 airfoil.

	Present study	Exp. results (Lien & Kalitzin, 2001)	Numerical results (Lien & Kalitzin, 2001)
Number of grid nodes	42,000	–	32,768
Cl	.803	.803	.803
Cd	.0169	.0167	.0169

given in Lien and Kalitzin (2001) are respectively presented in Table 3 and Figure 6, and show an acceptable accuracy. The value of y^+ over this airfoil is always less than 1.4.

To model the suction or the blowing, as shown in Figure 7, a channel is used over the airfoil surface and using a pressure difference between its inlet and outlet, the flow is sucked in or blown out of the airfoil. The channel geometry includes three main parameters: $x_{s/b}$, $L_{s/b}$ and $\Theta_{s/b}$. $x_{s/b}$ denotes the distance between suction/blowing initial point and the leading edge. $L_{s/b}$ is the length of entrance channel (these two parameters are non-dimensionalised with airfoil chord). $\Theta_{s/b}$ is the suction/blowing inclination angle.

For validation of our simulation scheme to predict performance of our suction/blowing models, a NACA-64A010 airfoil with suction parameters, $x_{s/b}$ = .69c, $L_{s/b}$ = .025c introduced in Mazaheri and Nejati (2015) is numerically analysed and results are compared with experimental results presented in Qin et al. (2004). For suction and blowing optimisation, we select the following ranges of design variables:

$$\begin{cases} .3c \le x_{s/b} \le .65c & \text{for suction} \\ .6c \le x_{s/b} \le .9c & \text{for blowing} \\ .005c \le L_{s/b} \le .03c \end{cases} \tag{5}$$

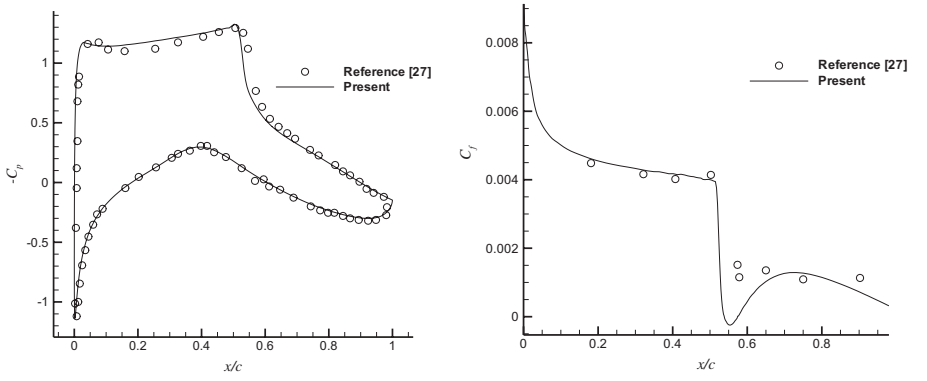

Figure 6. The pressure and the skin friction coefficient distribution over the RAE-2822 airfoil.

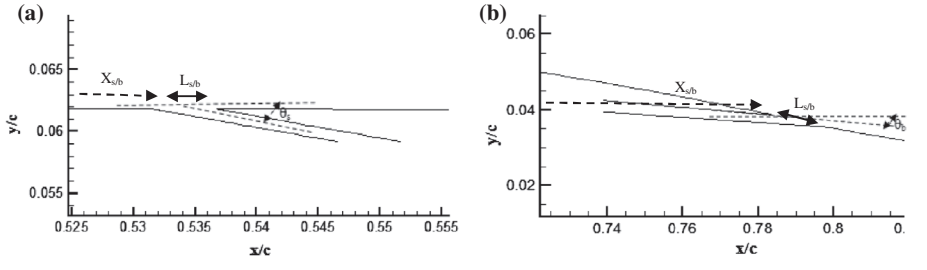

Figure 7. The geometry of suction/blowing used in our optimisation procedure. (a) the suction, (b) the blowing.

7. Modelling the bump geometry

In this research, the sine function with minor improvement with respect to Tian et al. (2011) is used to model the bump geometry. The Hicks-Henne (Equation (6)) is a sine function that is able to create bumps with different heights, slopes, asymmetries and lengths. One of the features of this function is that the slope of formed curvature is equal to zero at both ends ($f'(0) = f'(1) = 0$). This characteristic prevents any discontinuity formation between the airfoil and the bump. Equation (6) describes the Hicks-Henne function. In this equation, h_B is the maximum bump height, t represents the slope parameter and x represents the non-dimensional length parameter with respect to bump length (l_B). All the geometrical details are shown in Figure 8.

$$f(x) = h_B\left(\sin\left(\pi x^m\right)\right)^t,\ 0 \le x \le 1 \tag{6}$$

In Equation (6), the parameter m defined by Equation (7) is used to create asymmetric bumps. Here, C_B/l_B represents the degree of asymmetry and is in the range of (0,1), see Figure 8. $C_B/l_B = .5$ represents a symmetric bump.

$$m = \frac{\ln(.5)}{\ln(c_B/l_B)} \tag{7}$$

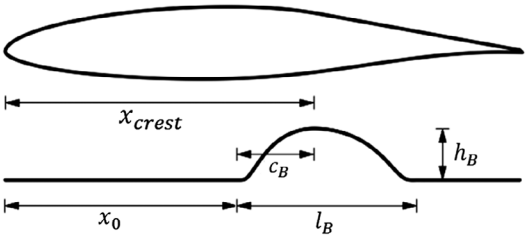

Figure 8. Design parameters for optimisation of the 2D bump.

The other important parameter is x_0, the beginning of the bump on the airfoil surface (Figure 8). The ranges of variation for the bump geometry parameters are given below (all the variables are non-dimensionalised with respect to the airfoil chord length).

$$\begin{cases} 0 \le h_B \le .01\text{c} \\ .3 \le x_0/l_B \le .55 \\ .4 \le c_B/l_B \le .85 \\ .5 \le t \le 2 \\ .15 \le l_B \le .3 \end{cases} \tag{8}$$

8. Separate multi-point optimisation of bump, suction and blowing on airfoils

To reduce the drag coefficient, we use multi-point optimisation algorithm to find optimised values for design parameters of each of bump, suction and blowing applied separately to the airfoil. The cost function is assumed as:

$$F = \sum_{k=1}^{N} Cd_k. \tag{9}$$

where N is the number of optimisation points or flight conditions. In this algorithm, for all flight conditions, we first solve the flow field and adjoint equations. The total gradient is finally computed as the summation of gradients in all flight conditions (for more details see Jameson et al. [2007]). The algorithm is converged when the summation is close to zero, which means that the geometry in each point is the best possible in view of decreasing the cost function.

The design parameters for the bump and for the suction/blowing, along with their ranges of variation are described in Equations (5) and (8), respectively. First, we solve a multi-point optimisation problem to optimise all five design parameters of a SCB for an RAE-5225 airfoil, for a range of off-design flight conditions stated in Table 1. Results are shown in Tables 4 and 5. A similar multi-point optimisation problem has been solved by authors for a SCB over an RAE-2822 airfoil in

Table 4. Geometry of the 2D multi-point optimised bump for the RAE-5225 airfoil.

SCB	x_0/c	c_B/c	t	l_B/c	h_B/c
Initial value	.5	.5	1.0	.2	.0
Optimised value	.423	.591	1.03	.296	.00531

Table 5. Results of the multi-point optimisation for the RAE-5225 airfoil with an optimised SCB.

Flight condition	M	Cl	Cd	L/D	$\%\Delta Cl$	$-\%\Delta Cd$	$\%\Delta L/D$
1	.74	.718	.0162	44.3	3.48	8.99	13.9
2	.75	.693	.0187	36.3	2.21	10.5	12.0
3	.76	.652	.0217	30.0	1.08	10.3	12.8
4	.77	.601	.0247	24.3	.502	9.85	11.5

Table 6. Geometry of the multi-point optimised bump for the RAE-2822 airfoil (Mazaheri et al., 2015).

SCB	x_0/c	c_B/c	t	l_B/c	h_B/c
Initial value	.5	.5	1.0	.2	.0
Optimised value	.534	.535	1.23	.298	.00713

Table 7. Results of the multi-point optimisation for the RAE-2822 airfoil with an optimised SCB (Mazaheri et al., 2015).

Flight condition	M	Cl	Cd	L/D	$-\%\Delta Cd$	$\%\Delta L/D$
1	.75	.546	.0133	41.1	.150	−1.25
2	.76	.576	.0140	41.2	12.8	21.9
3	.78	.498	.0195	25.5	12.1	16.3
4	.79	.448	.0223	20.1	11.5	13.6

Mazaheri, Nejati et al. (2015), with five design parameters, and results are repeated here in Tables 6 and 7. This solution will be used for our comparative analysis.

Comparison of data in Tables 1 and 5 shows that the optimised SCB improves average performance of the RAE-5225 about 12.5% and the improvement is almost uniform in the range of Mach number variation. However, for the RAE-2822 the average improvement is about 12.7%, but it is very non-uniform, including performance loss in the first flight condition.

All flow control methods have two different aerodynamic effects: a viscous interaction with the boundary layer (near field effects) and an inviscid interaction with the outer flow (far field effects). To study the near field effects, in Figure 9, the pressure coefficient distribution for the RAE-5225 with a multi-point optimised SCB at different flight conditions is compared with the clean airfoil. The main observation here is that, while we have one strong shock wave over the original airfoil, it is restructured to a weakened shock wave in the multi-point case.

One clearly observes that the clean airfoil experiences a three-wave structure; expansion waves, followed by a non-isentropic shock wave, and an isentropic compression region. The SCB changes the flow structure to a five-wave model; expansion waves followed by isentropic compression waves, another expansion

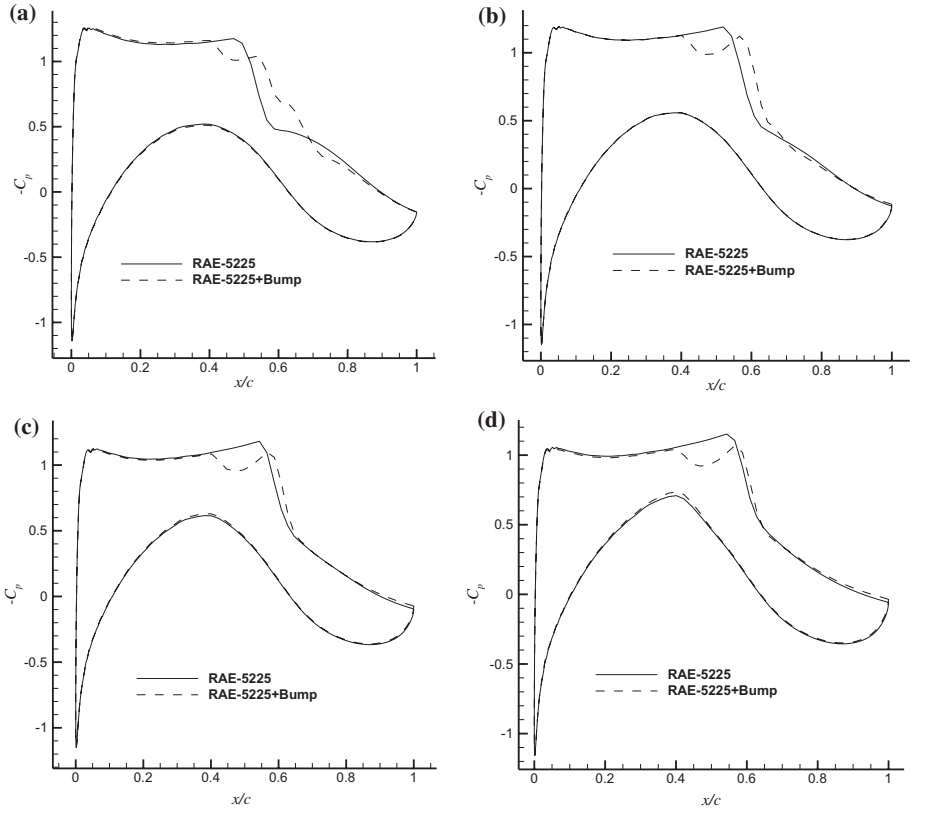

Figure 9. The pressure coefficient distribution around the RAE-5225 airfoil with and without SCB at (a) $M_\infty = .74$ (b) $M_\infty = .75$ (c) $M_\infty = .76$ (d) $M_\infty = .77$.

waves (most times missing), and then a weak shock wave and a compression region. The main observation here is that, while there is one strong shock wave over the clean airfoil, it is resolved to two compression waves (including a fairly isentropic compression and a weak shock wave) in the multi-point case. The physical basis of bump aerodynamic advantage relies on this wave structure, i.e. the isentropic compression waves generated after the initial expansion waves do not allow the abrupt pressure drop which will trigger a strong shock wave over the airfoil.

After optimisation of the SCB, two similar multi-point optimisation problems are solved separately for the suction and the blowing. Initially, the suction and blowing region are located upstream and downstream of the shock wave, respectively. The suction angle with respect to the chord is fixed at −10° for both airfoils and the blowing is fixed at 0° for the RAE-5225 and at −5° for the RAE-2822. The initial and final values of design parameters for both airfoils are given in Table 8.

The aerodynamic performance of the both original airfoils, and airfoils with each of these three different flow control methods, all with optimum values of design parameters are shown in Figures 10 and 11. One observes that both blowing

Table 8. Design variables for the multi-point optimisation of the suction or the blowing for both airfoils.

	$x_{s/b}/c$	$L_{s/b}/c$
Initial value (Suction)	.450	.010
Optimised value (Suction) RAE-5225	.306	.00614
Optimised value (Suction) RAE-2822	.385	.00534
Initial value (Blowing)	.850	.010
Optimised value (Blowing) RAE-5225	.683	.0223
Optimised value (Blowing) RAE-2822	.788	.0202

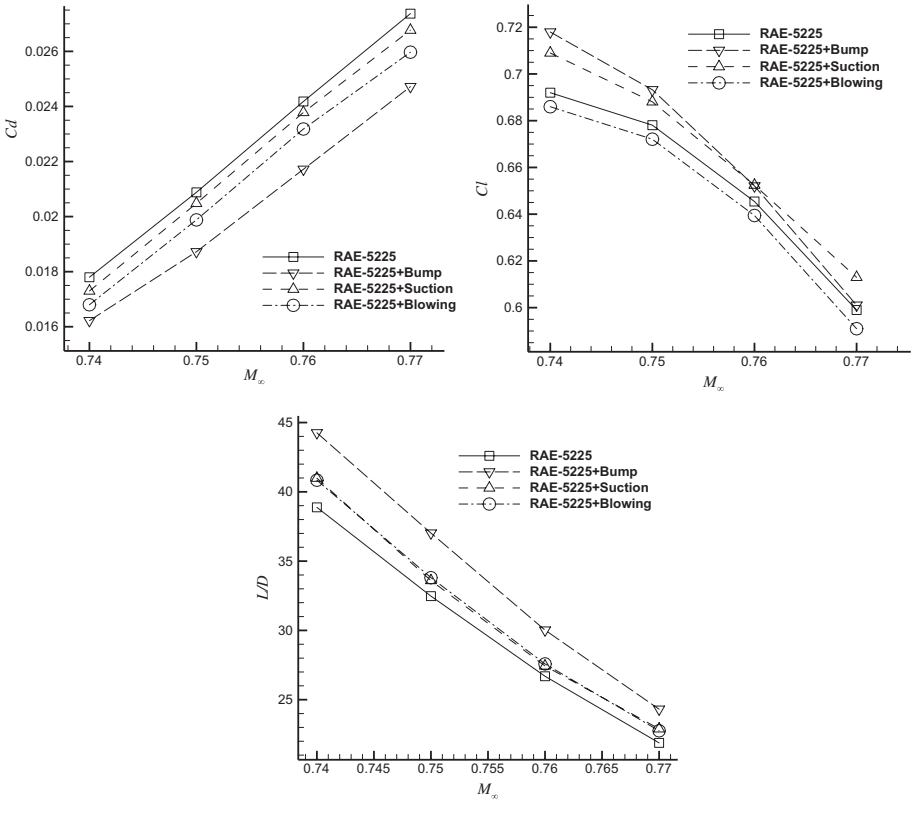

Figure 10. Comparison of the multi-point optimisation results for the RAE-5225 airfoil with only one flow control: the suction or the blowing or the bump.

and suction have improved the aerodynamic performance in all flow conditions, while the performance of the bumped airfoil is usually better than the clean airfoil. The blowing decreases the lift coefficient in lower Mach numbers but the drag decrement by the blowing is more than the suction. The average performance improvement for bumped airfoil is significantly better than the other two methods, and this value for the blowing method is slightly better than the suction. The average relative performance improvement in comparison with the clean airfoil for the RAE-5225 for the bump, the suction and the blowing is 11.7, 4.16, and 4.21%, respectively, and these figures are 11.1, 4.04, and 6.61% for the RAE-2822.

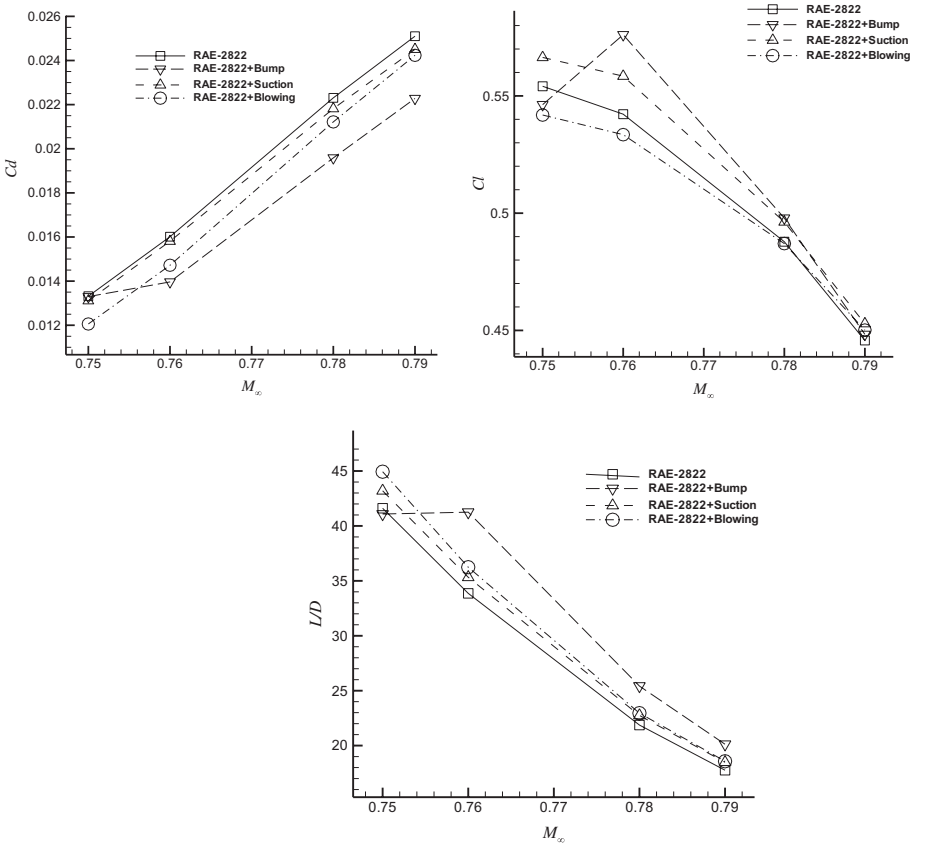

Figure 11. Comparison of the multi-point optimisation results for the RAE-2822 airfoil with only one flow control: the suction or the blowing or the bump.

Tables 9 and 10 show the initial and the final values of the mass flux and the specific momentum for suction and blowing of the RAE-2822. One observes that the mass flux and the specific momentum of the flow control methods in optimised shapes similarly increase or decrease (with a slight exception at the first point in the blowing case). It shows that both of them are activated or deactivated based on the strength and location of the shock waves.

Figure 12 compares the pressure coefficient distribution for optimised suction or blowing with those of the clean airfoil at flight condition 2 for the RAE-2822. Due to supersonic nature of the flow around the suction inlet, the pressure distribution in the suction inlet is discontinuous, but near the blowing outlet we have a smooth pressure difference. The suction has resulted in a pressure reduction after its inlet, but we have an increase in pressure before the blowing outlet. The suction does not change the shock wave strength and position, while the blowing has increased the displacement thickness, and has moved the shock wave towards the leading edge resulting in a weaker shock wave.

Table 9. Mass flow and average velocity in multi-point optimisation of the suction for the RAE-2822 airfoil.

M_∞	C_Q-initial	C_Q-final	U_{ave}/U_∞-initial	U_{ave}/U_∞-final
.75	−.000346	−.0000477	.861	.527
.76	−.000301	−.0000504	.850	.539
.78	−.000311	−.0000561	.868	.559
.79	−.000312	−.0000521	.842	.544

Table 10. Mass flow and average velocity in the multi-point optimisation of the blowing for the RAE-2822 airfoil.

M_∞	C_Q-initial	C_Q-final	U_{ave}/U_∞-initial	U_{ave}/U_∞-final
.75	.000445	.000607	.309	.423
.76	.000471	.000624	.317	.418
.78	.000573	.000718	.361	.433
.79	.000651	.000772	.398	.459

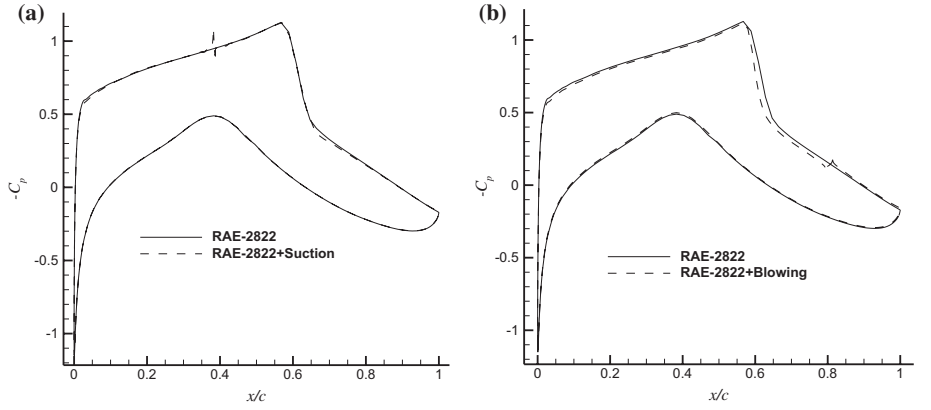

Figure 12. The pressure coefficient distribution over the RAE-2822 airfoil at flight condition 2: (a) with suction, (b) with blowing.

Figure 13 shows the skin friction distribution for the upper surface of the RAE-5225 airfoil in the fourth flight condition (a) with suction (b) with blowing. The suction has decreased the boundary layer thickness both before and after the shock wave, while the blowing has energised the boundary layer and has decreased its thickness after $x/c = .7$ till the trailing edge. Obviously both of them have increased the skin friction.

Figure 14 shows the streamlines and the pressure contours around the suction and the blowing outlet at flight condition 3 for The RAE-2822 and compares them with the clean and the bumped airfoil. For the RAE-2822 with the SCB, the flow pattern over the airfoil is initiated with expansion waves, and then the isentropic compression waves are formed at the uphill of the bump. After the bump crest point, a weak expansion occurs, and finally a weakened shock wave happens and is followed by more isentropic compression waves. We have also a small

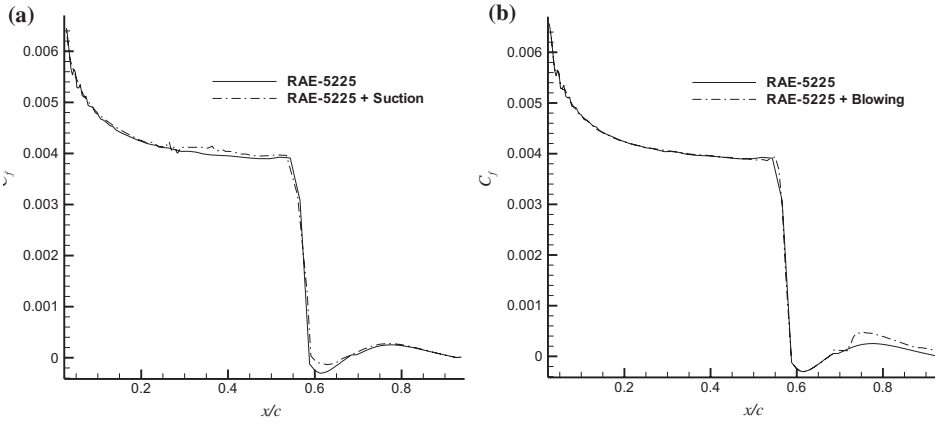

Figure 13. The skin friction coefficient distribution over the RAE-5225 upper side at flight condition 4: (a) with suction (b) with the blowing.

separation zone after the bump. Unlike the five-wave pattern (**E**-**IC**-**E**-**NC**-**IC**, see Mazaheri, Nejati et al. [2015] for details) generated by the SCB, the suction and the blowing generate a three-wave (**E**-**NC**-**IC**) pattern, i.e. some expansion waves, then a compressive shock wave, followed by some isentropic compression waves (Figure 14(c) and (d)).

To study the boundary layer interactions with the suction and the blowing for flight condition 4 which involves the strongest interactions, the velocity profile is depicted in six stations over the RAE-2822 in Figure 15. Initially at $x/c = .65$ and $x/c = .7$ the suction has the thinnest boundary layer. Later on, the blowing energises the boundary layer (Figure 15(d)), and its final boundary layer thickness (Figure 15(e) and (f)) is less than that of the original airfoil and the case with suction.

9. Multi-point optimisation of simultaneous suction and blowing (without bump)

Here we investigate the simultaneous optimisation of suction and blowing on both airfoils. The suction and the blowing angles are fixed as before. The number of design variables is four, two for suction location and its inlet width, and two for the blowing. The multi-point optimisation results are given in Table 11. Subscript *s* denotes suction and *b* denotes blowing.

Figure 16 compares the aerodynamic performance coefficients of using a single flow control method (i.e. the suction or the blowing) with the hybrid usage for the RAE-5225. Figure 17 does similarly for the RAE-2822 airfoil. Note that the cost function is again the drag coefficient. We do not observe improvement in the lift coefficient at any flight condition for the RAE-2822, but the *Cl* is improved at all flight conditions for the RAE-5225 airfoil. Both the drag coefficient and the aerodynamic efficiencies are improved at all flight conditions for both airfoils. However, the improvements in aerodynamic efficiencies are not significant, and are about 8% for both airfoils in comparison with the clean airfoils.

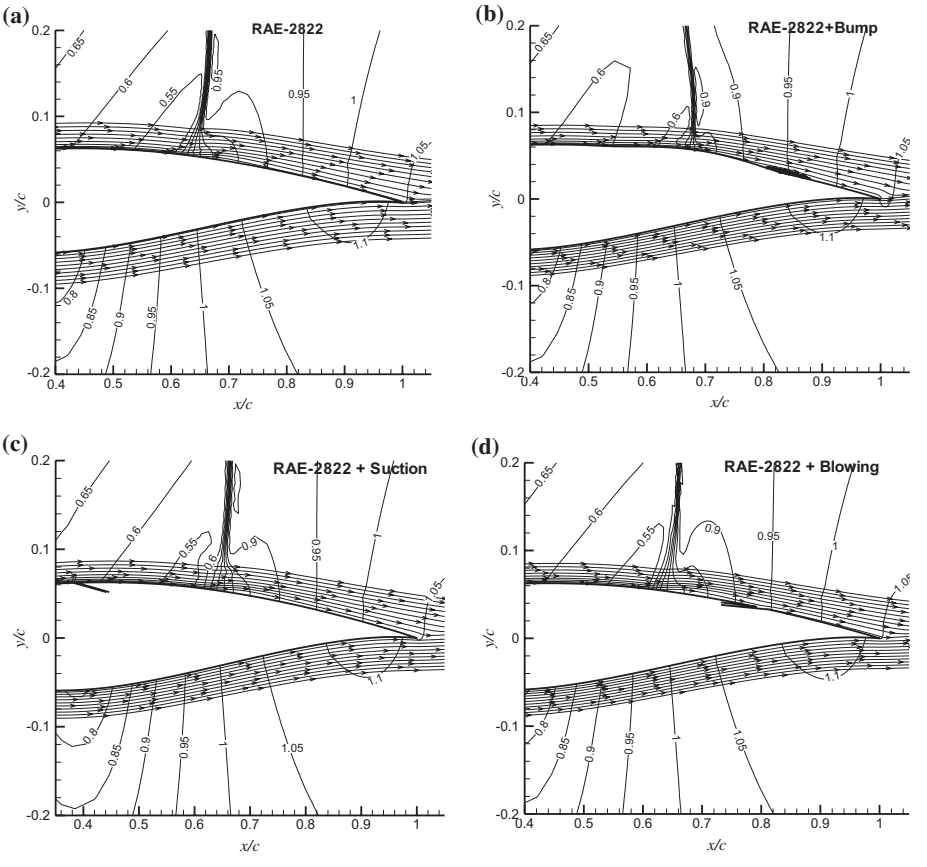

Figure 14. The streamlines and the pressure contours over the RAE-2822 airfoil at flight condition 3: (a) clean airfoil, (b) with bump, (c) with suction, (d) with blowing.

Figure 18 compares the pressure coefficient distribution for the RAE-5225 with simultaneous optimisation of suction and blowing with those of the clean airfoil at flight condition 3. Due to supersonic nature of the flow around the suction inlet, the pressure distribution in the suction inlet is discontinuous, but near the blowing outlet, we have a smooth pressure difference. According to this figure, the blowing has moved the shock wave a little towards the leading edge. Figure 19 compares the skin friction coefficient distribution around the shock wave position, with the original clean airfoil at flight condition 4 for both airfoils. According to this figure, the separated region after the shock wave for the RAE-2822 is completely removed by the effective suction and blowing and it is largely removed for the RAE-5225 case.

10. Simultaneous multi-point optimisation of SCB, suction and blowing

Here we use all three flow control schemes together for both airfoils. We use nine design parameters for simultaneous optimisation of the SCB (five parameters), the

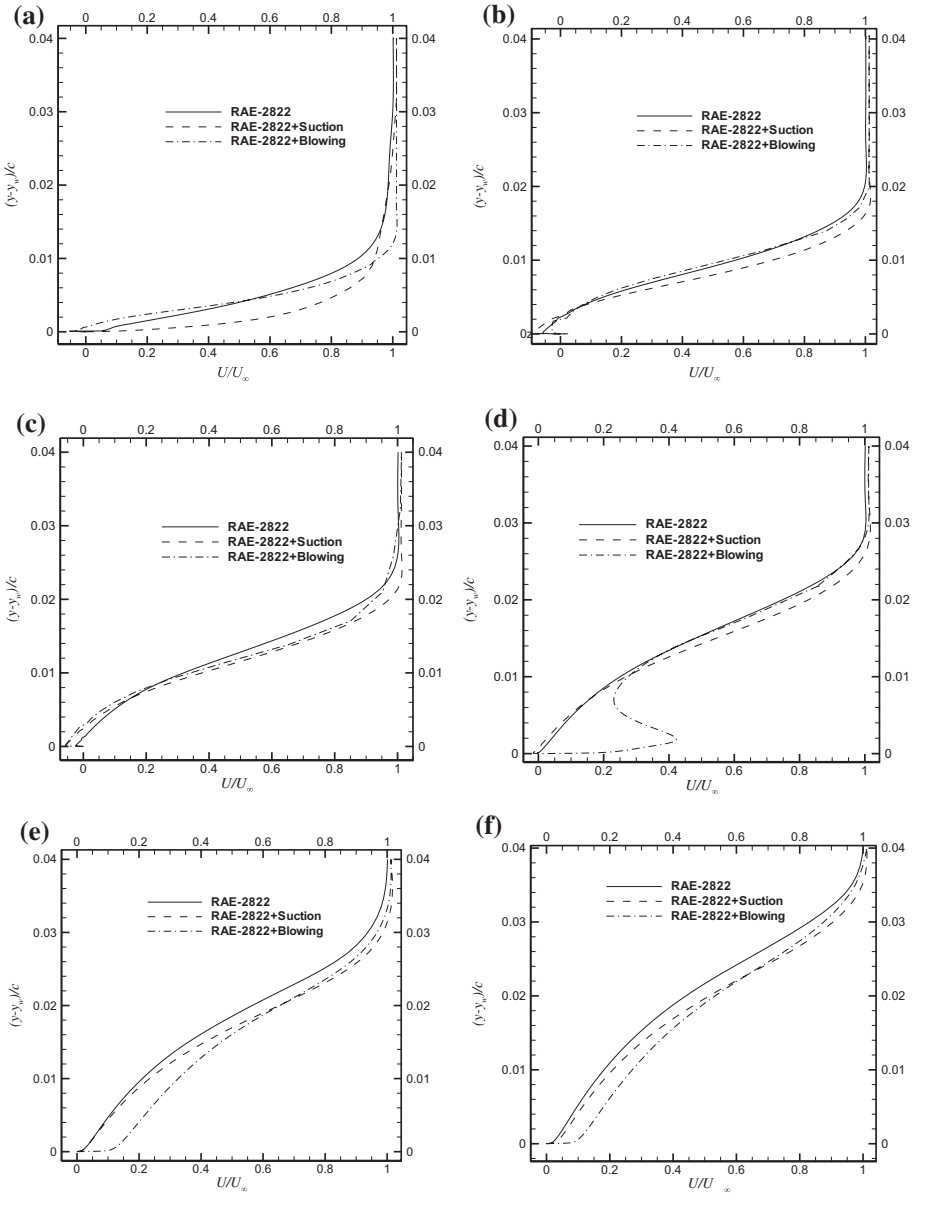

Figure 15. The boundary layer velocity profiles for the RAE-2822 airfoil with and without multi-point optimised flow control methods, at different locations: (a) $x/c = .65$, (b) $x/c = .70$, (c) $x/c = .75$, (d) $x/c = .80$, (e) $x/c = 85$, (f) $x/c = .90$.

Table 11. Design variables for the simultaneous multi-point optimisation of suction and blowing for both airfoils.

	x_s/c	L_s/c	x_b/c	L_b/c
Initial value	.450	.010	.850	.010
Optimised value RAE-5225	.313	.00673	.703	.0231
Optimised value RAE-2822	.388	.00596	.773	.0211

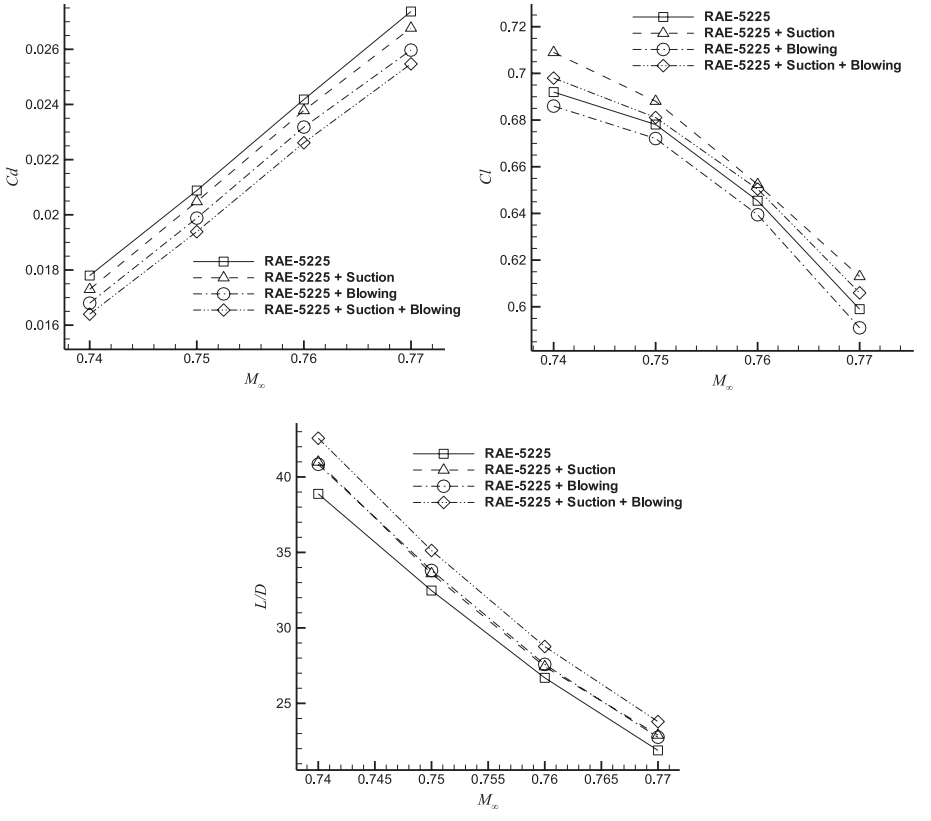

Figure 16. Comparison of the multi-point optimisation results for the RAE-5225 airfoil with simultaneous suction and blowing.

suction (two parameters) and the blowing (two parameters). The suction and the blowing angles are fixed again as before. All the other details of the optimisation procedure are as before. Table 12 gives the initial and the optimised values of the design parameters for both airfoils.

Figures 20 (for RAE-5225) and 21 (for RAE-2822) compare the aerodynamic coefficients of three cases: the original clean airfoil, the airfoil with the optimised SCB (based on Tables 4 and 6) and the airfoil with the optimised hybrid flow control methods. Since in the multi-point optimisation we find the best solution for a range of flight conditions, it may not have the best performance at all points. The average performance improvements with respect to the clean airfoil for *Cd*, *Cl*, and *L/D* are respectively 13.9, 1.18 and 17.7% for the RAE-5225 airfoil with complete hybrid optimised flow controls and these average improvements are, respectively, 19.6, –.0771 and 22.1%, for the RAE-5225 airfoil. The drag coefficient and the aerodynamic efficiency for the hybrid flow control method is always better than both clean airfoils, while the lift coefficient is decreased for the optimised airfoil at the first and second points in RAE-2822 case. In general, qualitative comparison of these results with previous works of Mazaheri and Nejati (2015),

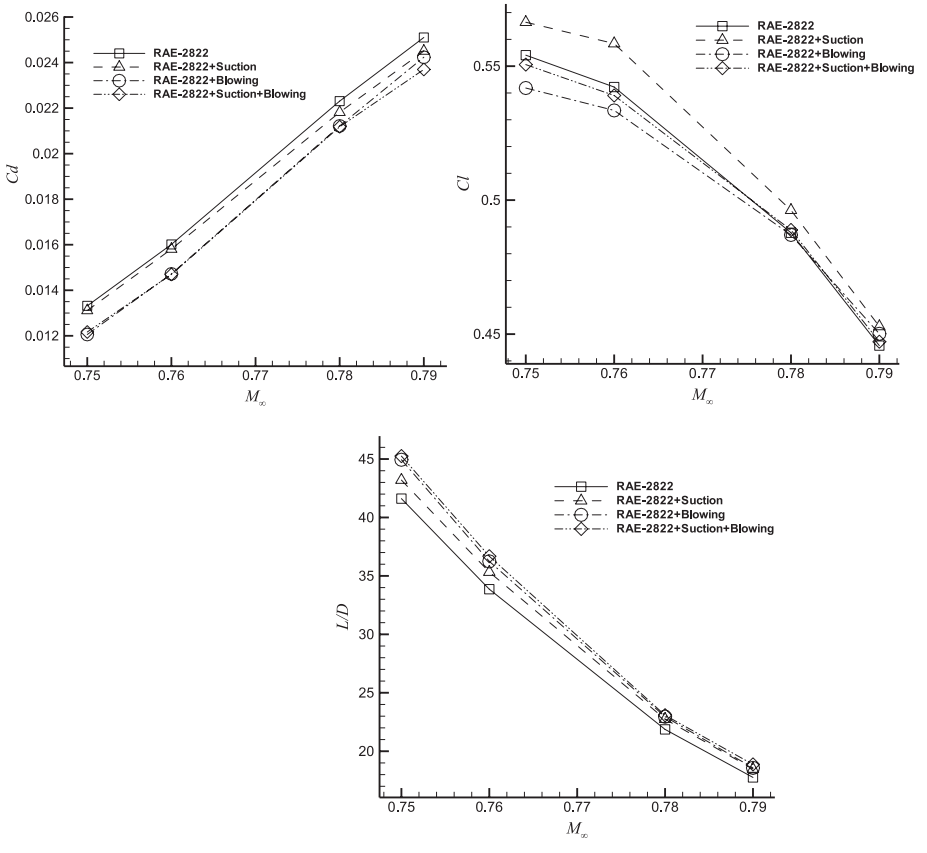

Figure 17. Comparison of the multi-point optimisation results for the RAE-2822 airfoil with simultaneous suction and blowing.

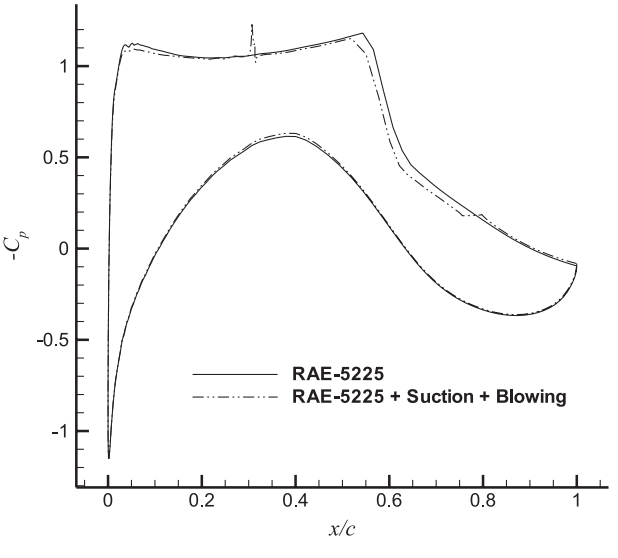

Figure 18. Comparison of the pressure coefficient distribution over the RAE-5225 airfoil at flight condition 3 with simultaneous suction and blowing with the clean airfoil.

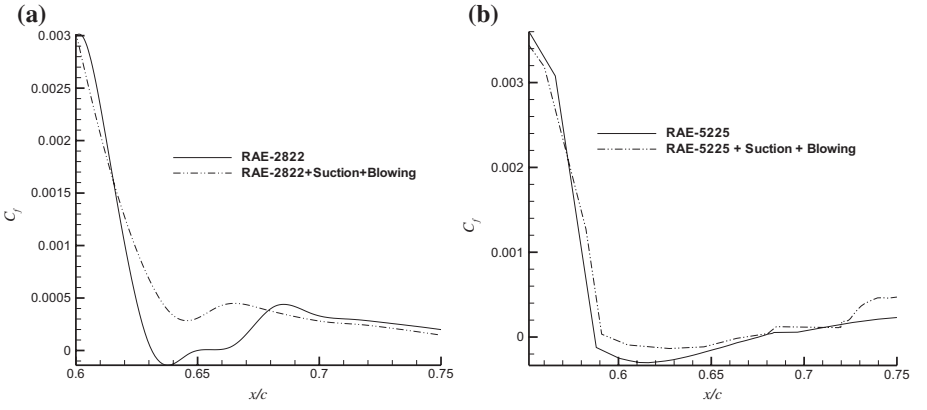

Figure 19. The skin friction coefficient distribution around shock wave position at flight condition 4: for (a) the RAE-2822 (b) the RAE-5225.

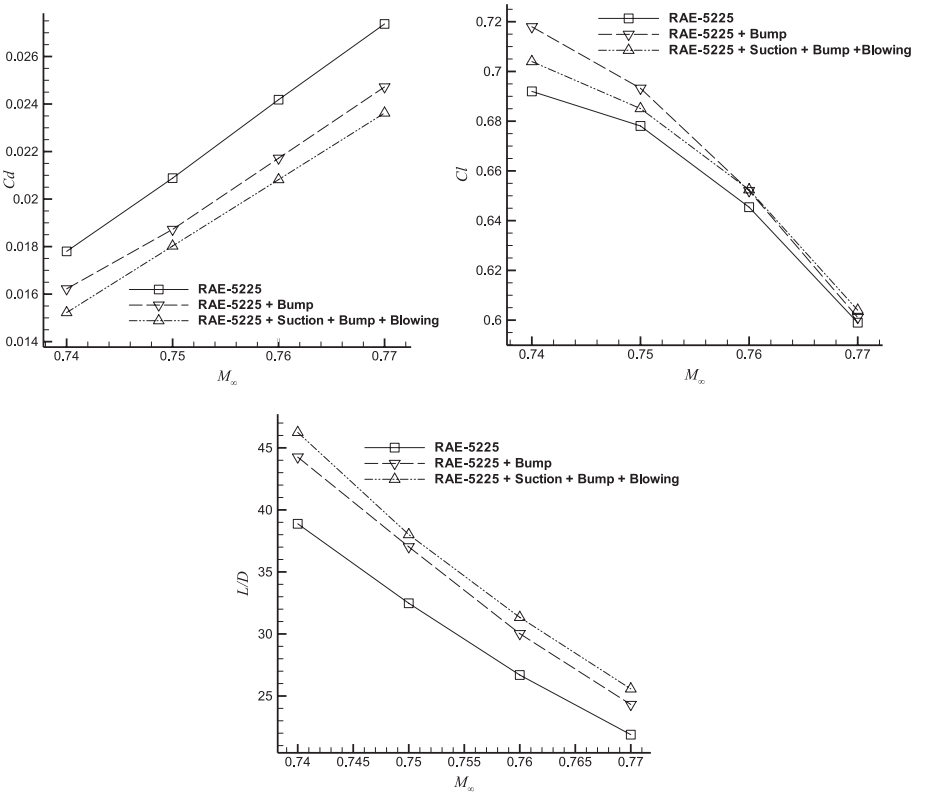

Figure 20. Comparison of the aerodynamic coefficients and efficiencies of the simultaneous multi-point optimisation of bump, suction and blowing with bumped and un-bumped RAE-5225 airfoil.

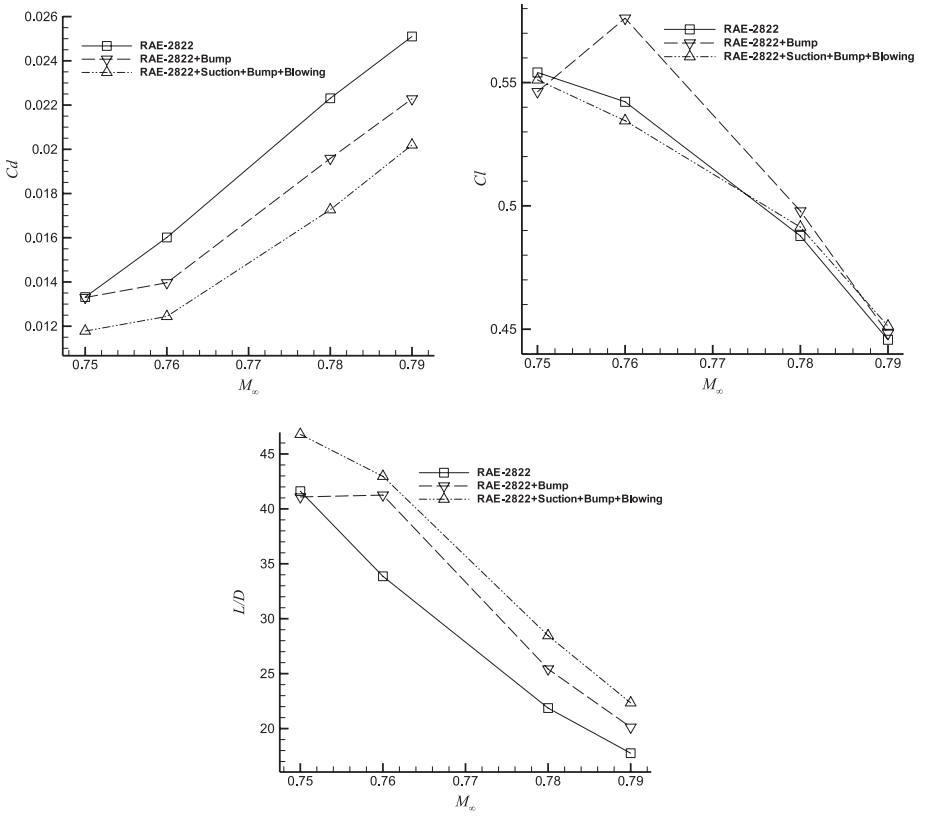

Figure 21. Comparison of the aerodynamic coefficients and efficiencies of the simultaneous multi-point optimisation of bump, suction and blowing with bumped and un-bumped RAE-2822 airfoil.

Table 12. Design variables for the simultaneous multi-point optimisation of bump, suction and blowing for both airfoils.

	x_s/c	x_b/c	L_s/c	L_b/c	x_0/c	c_B/c	t	l_B/c	h_B/c
Initial value	.450	.850	.010	.010	.500	.500	1.00	.200	.000
Optimised value RAE-5225	.397	.662	.00647	.0222	.431	.593	1.06	.294	.00587
Optimised value RAE-2822	.538	.753	.00576	.0193	.506	.598	1.11	.299	.00614

Mazaheri, kiani et al. (2015) and Mazaheri, Nejati et al. (2015) shows that using a much stronger methodology, results are significantly improved in comparison with previous works.

Obviously many other options are available for the cost function which may result in slightly different solutions. Summary of the results are given in Tables 13 and 14. Obviously, the last row is about the summation of the other two rows. If we use the constant lift constraint, the third row will not change significantly.

To better understand the physical reasons for these significant improvements, Figure 22 shows the streamlines and the pressure contours around the RAE-5225

Table 13. Average improvements of the aerodynamic coefficients and efficiencies over the studied range of off-design Mach numbers for the RAE-5225.

	Clean airfoil	Bump	Suction	Blowing	Suction + blowing	Bump + suction + blowing
$\%\Delta Cl$	0	2.01	1.83	−.994	.803	1.18
$-\%\Delta Cd$	0	9.82	2.11	4.86	7.05	13.9
$\%\Delta L/D$	0	11.7	4.16	4.21	8.61	17.7

Table 14. Average improvements of the aerodynamic coefficients and efficiencies over the studied range of off-design Mach numbers for the RAE-2822.

	Clean airfoil	Bump	Suction	Blowing	Suction + blowing	Bump + suction + blowing
$\%\Delta Cl$	0	1.91	2.17	−.856	−.206	−.0775
$-\%\Delta Cd$	0	9.92	1.95	5.87	6.52	19.6
$\%\Delta L/D$	0	11.1	4.04	6.61	7.63	22.1

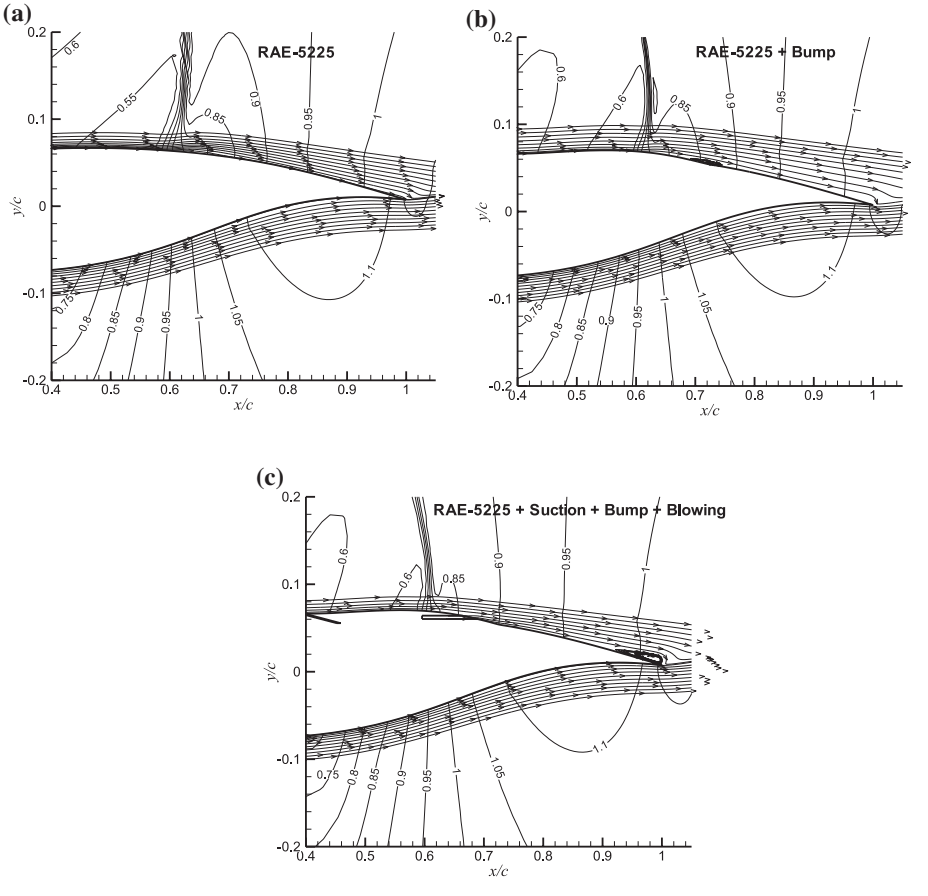

Figure 22. The streamlines and the pressure contours over the RAE-5225 airfoil at flight condition 4: (a) clean airfoil, (b) with bump (c) with bump + suction + blowing.

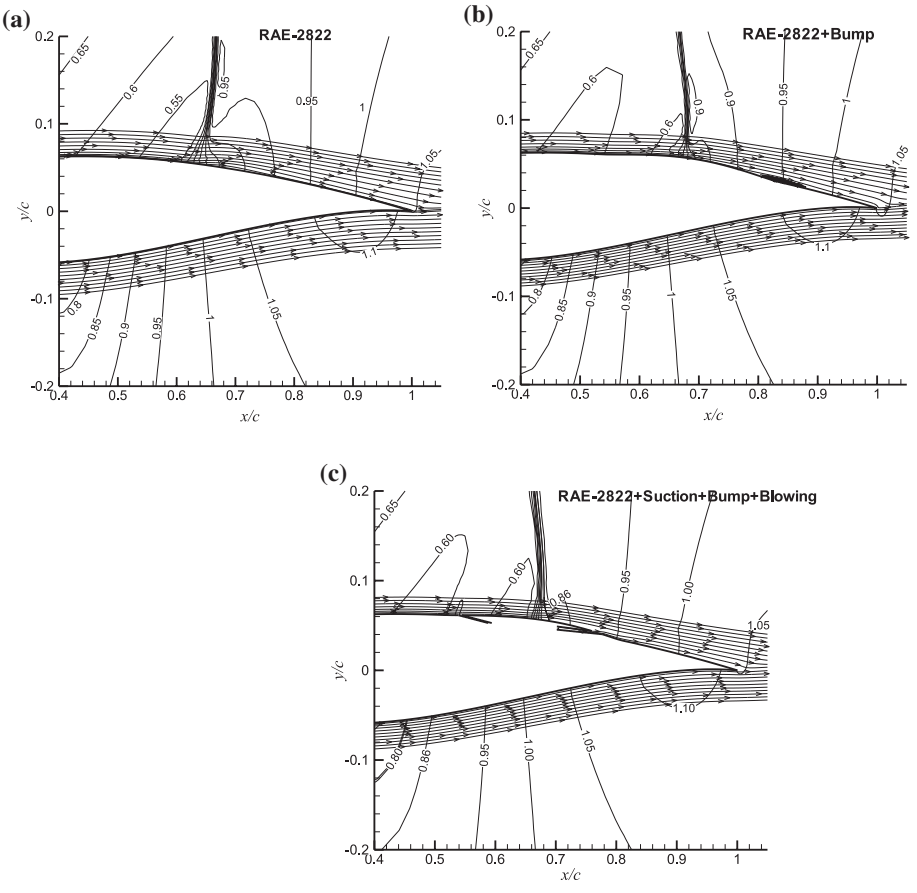

Figure 23. The streamlines and the pressure contours over the RAE-2822 airfoil at flight condition 3. (a) clean airfoil, (b) with bump (c) with bump + suction + blowing.

airfoil at flight condition 4, which involves the highest SWBLI. Figure 22 compares the results for all the above three cases, i.e. the original clean airfoil, the optimised bumped airfoil (based on Table 4) and the airfoil with complete hybrid flow controls. For the bumped airfoil, the shock wave is clearly weakened, but there is a small separation zone after the bump. When using hybrid flow control, the shock wave is weakened, and the separation zone after the bump is also reduced and moved to a slight portion of the trailing edge.

Figure 23 similarly shows the streamlines and the pressure contours around the RAE-2822 airfoil, but at flight condition 3. Again we compare the results for all the above three cases, the original clean airfoil, the optimised bumped airfoil (based on Table 6) and the airfoil with complete hybrid flow controls. Again, for the bumped airfoil, the shock wave is clearly weakened, but the flow is separated after the bump. When using hybrid airfoil, the shock wave is weakened, and the separation zone after the bump is completely removed. Comparison of Figures 22

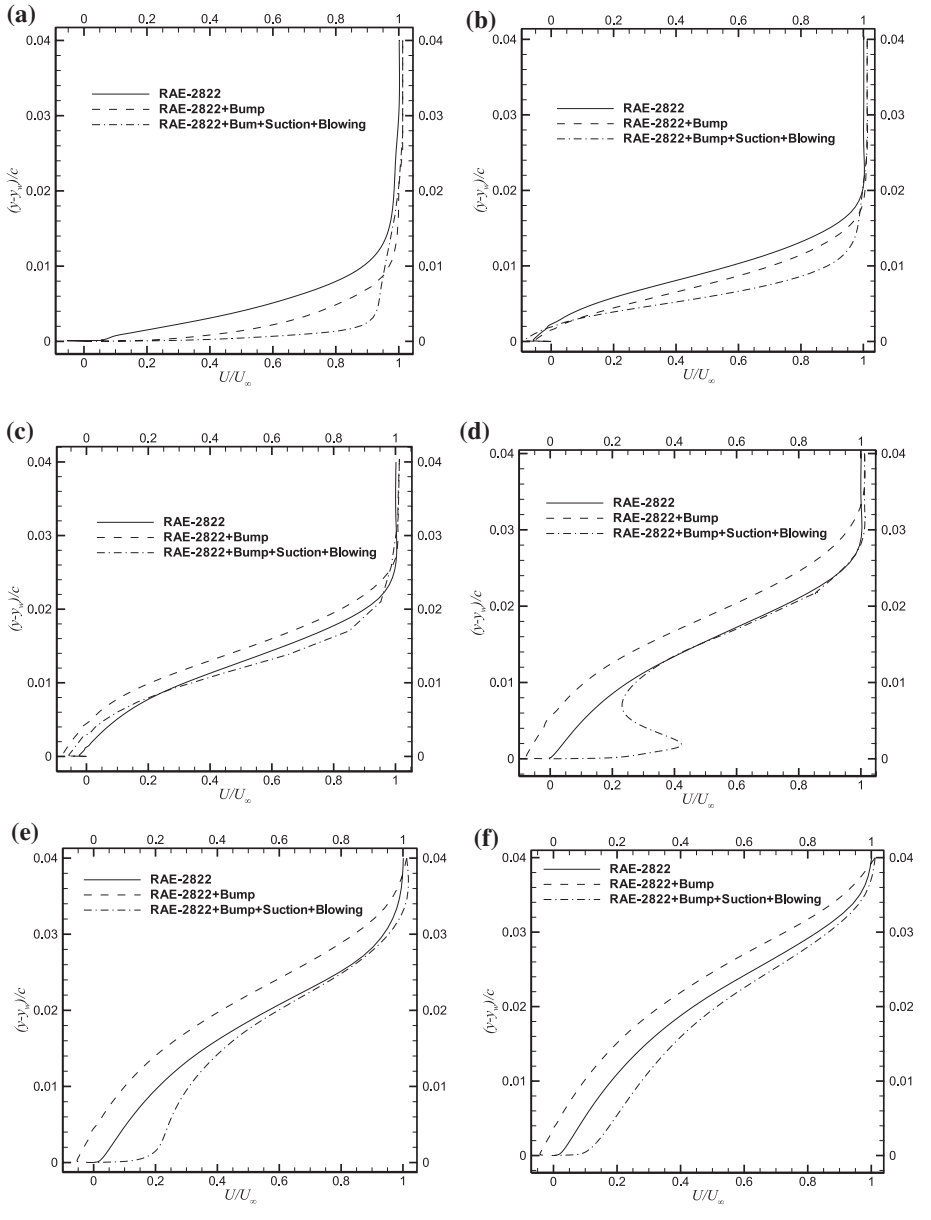

Figure 24. The boundary layer velocity profiles for the RAE-2822 airfoil with and without multi-point optimised flow controls, at different locations. (a) $x/c = .65$, (b) $x/c = .70$, (c) $x/c = .75$, (d) $x/c = .80$, (e) $x/c = 85$, (f) $x/c = .90$.

and 23 convinces us that results reported in this article are probably qualitatively valid for most transonic airfoils.

Finally to study the interactions between the shock wave and the boundary layer, and also to investigate the boundary layer structure at flight condition 4 for the RAE-2822 airfoil, the velocity profiles at six different stations around and after the shock wave are depicted in Figure 24. At this flight condition, we have the

strongest interactions. Note that the hybrid airfoil has always a thinner boundary layer than the original airfoil, while the optimised bumped airfoil results in a huge separated region, and a thicker boundary layer after $x/c = .75$. The blowing at $x/c = .75$ in the hybrid airfoil inserts enough momentum into the boundary layer, prevents separation and decreases the boundary layer thickness effectively.

11. Conclusions

In this research, we investigated how multi-point optimisation of three different flow control schemes may affect the wave structure and improve the aerodynamic performance and the SWBLI over the RAE-5225 and the RAE-2822 supercritical airfoil. The multi-point optimisation procedure used here, assuming constant angle of attack, provides the best possible shape and location for a range of off-design transonic Mach numbers. We have first studied the application of suction or blowing alone and compared the results with an optimised bumped airfoil. Then we have considered the suction and the blowing together over the clean airfoil. Finally we have considered optimisation of the airfoil with the fully hybrid flow control methods.

Tables 13 and 14 provide quantitative comparison of all cases considered in this article. Using a single flow control, the SCB is the most effective, with more than 11% improvement in the average aerodynamic efficiency for both airfoils, while the blowing is the second most effective. However, interestingly, because of non-linear physical interactions, for RAE-5225 the combination of the suction with the blowing is more effective than summation of their single usage. Obviously, the hybrid usage of all three methods provides the highest efficiency, which results in 17.7% improvement in the average aerodynamic efficiency for the RAE-5225 and 22.1% improvement for the RAE-2822. Results presented here convince us that conclusions reported in this article are probably qualitatively valid for most transonic airfoils. In general, qualitative comparison of these results with previous works of Mazaheri and Nejati (2015), Mazaheri, kiani et al. (2015), and Mazaheri, Nejati et al. (2015) show that introducing a much stronger methodology, using different flow controls, the aerodynamic performances are significantly improved in comparison with previous works.

Many interesting observations regarding the hydraulic features of the flow domain and the waves structure are also presented. We observed that usually the suction slightly decreases the boundary layer displacement thickness and does not change the shock wave strength and location, while the blowing increases the displacement thickness, and moves the shock towards the leading edge, resulting in a weaker shock wave. Also, the blowing along with the SCB effectively reduces or removes the separated region after the SCB.

List of symbols

$\mathbf{A}^T$	Jacobian of convective flux
c	Speed of sound
C_B/l_B	Bump degree of symmetry
Cd	Airfoil drag coefficient
C_f	Skin friction coefficient
Cl	Airfoil lift coefficient
C_p	Pressure coefficient
C_Q	Non-dimensional mass flow
ds	Surface element
E	Total energy per unit mass
f	Hicks-Henne Sine function
F	Cost function
$\mathbf{f}^{inv}$	Inviscid flux vector
$\mathbf{f}^{vis}$	Viscous flux vector
H	Total enthalpy
h_B	Maximum bump height
K	Turbulent kinetic energy
l_B	Bump length
L/D	Aerodynamic efficiency
M_∞	Free stream Mach number
Rey_∞	Free stream Reynolds number
t	Bump slope parameter
U_∞	Free stream velocity
$\mathbf{U}$	Vector of flow variable
u,v	Cartesian velocity component
V	Contravariant velocity
x,y	Cartesian coordinate system
x_0	Beginning of bump
Y^+	Non-dimensional wall coordinate
α	Airfoil angle of attack (AoA), deg
ρ	Density
ω	Turbulent specific dissipation rate

Note

1. Centre of Excellence in Aerospace Systems.

Disclosure statement

No potential conflict of interest was reported by the authors.

References

Anderson, W. K., & Venkatakrishnan, V. (1997). *Aerodynamic design optimization on unstructured grids with a continuous adjoint formulation*. In 35th Aerospace sciences meeting and exhibit, aerospace sciences meeting, AIAA Paper, 97–0643.

Ashill, P. R., Fulker, J. L., & Shires, A. (1992). A novel technique for controlling shock strength of laminar-flow aerofoil sections. In: *Proceedings 1st European forum on laminar flow technology* (pp. 175–183). Hamburg.

Balleur, J. C., Girodroux-Lavigne, P., & Gassot, H. (1999). *Prediction of transonic airfoil/wing flow with control using time-accurate viscous-inviscid interaction approach* (Results of Project EUROSHOCK II Supported by the European Union 1996–1999, 3rd Annual Report). Berlin: Springer. doi: 10.1007/978-3-540-45856-2_9

Bhattacharjee, S., Ahsan, M., Saha, M., & Mohammad, M. (2007). Numerical analysis of shock and boundary layer control over NACA0012 by contour bump, surface cooling and heating. In: *Proceedings of the international conference on mechanical engineering (ICME'07)* (pp. 29–31). Dhaka.

Birkemeyer, J. (1999). *Drag minimization on a transonic wing by ventilation and adaptive contour bump* (DLR Research Report 1999–28). Ph.D. Thesis University Hannover, Hannover.

Blazek, J. (2005). *Computational fluid dynamics: Principles and applications* (2nd ed.). Amsterdam: Elsevier.

Evans, M. R., Hynes, R. J., Norman, D. C., & Thomason, R. E. (1984). *Automatic flight control modes for the AFTI/F-111 mission adaptive wing aircraft*. AGARD-CP-384 (Vol. 25).

Jameson, A., Leoviriyakit, K., & Shankaran, S. (2007). *Multi-point aero-structural optimization of wings including planform variations*. 45th aerospace sciences meeting and exhibit, AIAA-2007-764, Reno.

Koenig, B., Paetzold, M., Lutz, T., & Kraemer, E. (2007). Shock control bumps on flexible a trimmed transport aircraft in transonic flow. *New Results in Numerical and Experimental Fluid Mechanics VI, 96*, 80–87. Berlin

Lee, D. S., Bugeda, G., Periaux, J., & Onate, E. (2013). Robust active shock control bump design using hyper parallel MOGA. *Computers & Fluids, 80*, 214–224.

Lien, F. S., & Kalitzin, G. (2001). Computations of transonic flow with v2-f turbulence model. *International Journal of Heat and Fluid Flow, 22*, 53–61.

Mazaheri, K., Kiani, K. C., Nejati, A., Zeinalpour, M., & Taheri, R. (2015). Optimization and analysis of shock wave/boundary layer interaction for drag reduction by shock control bump. *Journal of Aerospace Science and Technology, 42*, 196–208. doi: 10.1016/j.ast.2015.01.007

Mazaheri, F., & Nejati, A. (2015). The multi-point optimization of shock control bump with constant-lift constraint enhanced with suction and blowing for a supercritical airfoil. *International Journal of Flow, Turbulence and Combustion*, *96*, 639–666. doi: 10.1007/s10494-015-9671-8

Mazaheri, F., Nejati, A., & Kiani, K. C. (2016). Application of the adjoint multi-point and the robust optimization of shock control bump for transonic airfoils and wings. *International Journal of Engineering and Optimization*, *48*, 1887–1909. doi: 10.1080/0305215X.2016.1139811

Mazaheri, K., Nejati, A., kiani, K. C., & Taheri, R. (2015). The application of the gradient-based adjoint multi-point optimization of single and double shock control bumps for transonic airfoils. *International Journal on Shock Waves Detonations and Explosions, 25*. doi: 10.1007/s00193-015-0591-2

Mazaheri, K., & Zeinalpour, M. (2015). Entropy minimization in turbine cascade using continuous adjoint formulation. *Journal of Engineering Optimization*. doi 10.1080/0305215X.2014.998663

Menter, F. R., & Rumsey C. L. (1994). *Assessment of two-equation turbulence models for transonic flows*. 25th AIAA fluid dynamics conference, Colorado.

Milholen II, W. E., & Lewis, L. R. (2005). *On the application of contour bumps for transonic drag reduction*. AIAA 43rd aerospace sciences meeting and exhibit, AIAA-2005-0462, Reno.

Patzold, M., Lutz, T. H., Kramer, E., & Wagner, S. (2006). Numerical optimization of finite shock control bumps. In: *AIAA 44th aerospace sciences meeting and exhibit*, AIAA Paper 2006–1054 (pp. 9–12). Reno.

Qin, N., Zhu, Y., & Ashill, P. R. (2000). *CFD study of shock control at Cranfield*. 22nd international congress of aeronautical sciences, Harrogate.

Qin, N., Zhu, Y., & Shaw, T. H. (2004). Numerical study of active shock control for transonic aerodynamics. *International Journal of Numerical Methods for Heat & Fluid Flow, 14*, 444–466.

Ramezani, A., & Mazaheri, K. (2009). Multi-grid convergence acceleration for implicit and explicit solution of Euler equations on unstructured grids. *International Journal for Numerical Methods in Fluids*, inter science Wiley publication, *62*, 994–1012.

Rao, S. S. (1996). *Engineering optimization: Theory and practice* (3rd ed.). New York, NY: Wiley.

Stanewsky, E., Delery, J., Fulker, J., & de Matteis, P. (Eds.). (2002). Drag reduction by shock and boundary layer control. *Notes on Numerical Fluid Mechanics and Multi-disciplinary Design, 80*, 3–4.

Tian, Y., Liu, P., & Feng, P. (2011). Shock control bump parametric research on supercritical airfoil. *Science China, 54*, 2935–2944.

Vadillo, J. L., Agarwal, R. K., & Hassan, A. A. (2004). Active control of shock/boundary layer interaction in transonic flow over airfoils. Proceedings of the third international conference on computational fluid dynamics, ICCFD3 (pp. 361–366). Toronto, ON. Retrieved from http://link.springer.com/chapter/10.1007%2F3-540-31801-1_50

Yagiz, B., Kandil, O., & Pehlivanoglu, Y. V. (2012). Drag minimization using active and passive flow control techniques. *Aerospace Science and Technology, 17*, 21–31.